



HAL
open science

Microwave-assisted hydrothermal synthesis, characterization and catalytic performance of Fe-2(MoO4)(3) in the selective oxidation of propene

G. Hidalgo, M. Tonelli, L. Burel, M. Aouine, J. M. M. Millet

► To cite this version:

G. Hidalgo, M. Tonelli, L. Burel, M. Aouine, J. M. M. Millet. Microwave-assisted hydrothermal synthesis, characterization and catalytic performance of Fe-2(MoO4)(3) in the selective oxidation of propene. *Catalysis Today*, 2021, 363, pp.36-44. 10.1016/j.cattod.2019.05.021 . hal-03604554

HAL Id: hal-03604554

<https://hal.science/hal-03604554v1>

Submitted on 13 Feb 2023

HAL is a multi-disciplinary open access archive for the deposit and dissemination of scientific research documents, whether they are published or not. The documents may come from teaching and research institutions in France or abroad, or from public or private research centers.

L'archive ouverte pluridisciplinaire **HAL**, est destinée au dépôt et à la diffusion de documents scientifiques de niveau recherche, publiés ou non, émanant des établissements d'enseignement et de recherche français ou étrangers, des laboratoires publics ou privés.



Distributed under a Creative Commons Attribution - NonCommercial 4.0 International License

Microwave-assisted hydrothermal synthesis, characterization and catalytic performance of $\text{Fe}_2(\text{MoO}_4)_3$ in the selective oxidation of propene.

*G. Hidalgo, M. Tonelli, L. Burel, M. Aouine and J.M.M. Millet **

¹ Univ Lyon, Université Claude Bernard Lyon 1, CNRS, IRCELYON - UMR 5256, 2 Av.

Albert Einstein, 69626 Villeurbanne (France)

* Corresponding author: jean-marc.millet@ircelyon.univ-lyon1.fr

KEYWORDS : $\text{Fe}_2(\text{MoO}_4)_3$; microwave synthesis; heterogeneous oxidation catalyst;
structure sensitivity; selective propene oxidation; acrolein

ABSTRACT

A method for the simple and efficient microwave radiation-assisted hydrothermal synthesis of $\text{Fe}_2(\text{MoO}_4)_3$ has been developed. Several factors such as pH, addition rate, molybdenum precursor, type of solvent and various other microwave synthesis parameters are studied. The catalysts were characterized using X-ray diffraction, scanning electron microscopy, Mössbauer spectroscopy and specific surface area measurements. The results show that different morphologies can be obtained, depending on the conditions under which the iron molybdate is prepared. Nevertheless, in all cases the solid particles appear to be covered by an amorphous oxide layer, which is less rich in iron than in the case of a crystallized oxide layer. The presence of this amorphous layer was revealed on all facets of the molybdate, with approximately the same composition and thickness. In an effort to evaluate the relationship between the morphology of iron molybdate particles and their catalytic properties, several samples exhibiting different morphology were tested for the oxidation of propene to acrolein. These samples were tested for the oxidation of propene to acrolein. The catalysts with platelets morphology and exhibiting larger surface of (100) planes appeared more active. This was attributed to a faster re-oxidation due to the preferential diffusion of oxygen anions in the bulk structure channels perpendicular to these planes.

INTRODUCTION

Since the 1930s, iron molybdate ($\text{Fe}_2(\text{MoO}_4)_3$) has been known for its high activity and selectivity for the oxidation of methanol, and is still used on an industrial scale as a catalyst for the production of formaldehyde [1,2]. Iron molybdate has also been shown to be a particularly efficient catalyst for the oxidation of propene to acrolein when it is doped with tellurium, or as a photo-catalyst for the oxidative degradation of bromo-pyrogallol red [3-6]. Although iron molybdate is generally prepared by means of co-precipitation, or hydrothermal synthesis [6-8], it has recently been shown that microwave radiation can provide a straightforward and low-cost approach to the synthesis of this compound [6]. Furthermore, specific types of nanostructure can be obtained using this technique. Most of the catalytic oxidation reaction including the aforementioned one are running with the Mars and van Krevelen mechanism and are consequently structure sensitive. It is thus crucial to monitor the synthesis of oxidation catalysts, in order to control their texture and composition. In this respect, the study of MoO_3 , when used as a catalyst in the oxidation of propene to acrolein, provides a reference example. This particular reaction has been shown to be a suitable standard reaction for the study of structure dependence [9-13]. It has been shown that in the case of MoO_3 , propene is oxidized almost exclusively to acrolein on the (1 0 0) lateral face, and to CO_2 on the apical (1 0 -1), (1 0 1) and basal (0 1 0) planes of the catalyst [9,12]. Structure sensitivity has also been demonstrated on the same type of oxide, for other oxidation reactions such as the selective oxidation of but-1-ene and isobutene, and the oxidation of methanol [14-16].

The corresponding studies clearly demonstrate that the geometry of atomic arrangements at the oxide's surface is an important factor in the oxidation reactions. The relative extent of the various faces of a crystalline phase depends on the kinetic conditions

under which the crystal is grown and the growth of these faces is driven by complex laws, which in turn are strongly dependent on the method used to synthesize the catalyst. For this reason, the search for new preparation techniques, allowing oxide catalysts to be obtained with various morphologies, is still of considerable importance [17].

In the present study, a simple, rapid microwave irradiation route was used to synthesize pure $\text{Fe}_2(\text{MoO}_4)_3$ phases, with a controllable morphology and particle size. This technique was developed by exploring reaction parameters such as reaction time and temperature, as well as parameters related to the preparation of the starting solutions, including the pH of the solution, the source of iron or molybdenum, and the nature of the solvent. The influence of these parameters on the physico-chemical properties and the texture of the iron molybdates were studied, and the prepared solids were tested as catalysts for the oxidation of propene to acrolein. Tentative relationships between the oxides' catalytic properties and their structural and textural properties are established and discussed

EXPERIMENTAL

Chemicals used for the preparation and synthesis protocols

Iron nitrate hexahydrate ($\text{Fe}(\text{NO}_3)_3 \cdot 9\text{H}_2\text{O}$) (Ref. 254233), ammonium heptamolybdate ($(\text{NH}_4)_6\text{Mo}_7\text{O}_{24} \cdot 4\text{H}_2\text{O}$) (Ref. 1011810250), ethylene glycol (Ref. 324558), ethanol (Ref. 51976) and 2-methylpropan-1-ol (Ref. 1009841000) were purchased from Sigma-Aldrich chemical company. All reagents were analytical grade and used directly without further purification. Water was bi-distilled and gases for the catalytic testing were obtained from the laboratory internal gas distribution system. The catalyst was prepared by first mixing 10 ml

$\text{Fe}(\text{NO}_3)_3 \cdot 9\text{H}_2\text{O}$ solution 0.1021 M that was dropped into 10 ml $(\text{NH}_4)_6\text{Mo}_7\text{O}_{24} \cdot 4\text{H}_2\text{O}$ solution 0.0216 M with the addition rate controlled at 1-2-3 ml/min respectively using a SP100I syringe pump. The solution obtained corresponding to the suspension of a yellow precipitate was left 1 hour of magnetic stirring at 300 rpm and then transferred to a 30 ml reaction glass vial to perform the microwave treatment. The catalyst prepared with ethanol, 2-methylpropan-1-ol and ethylene glycol were synthesized in the same way but by adding 10 ml of a solution of $\text{Fe}(\text{NO}_3)_3 \cdot 9\text{H}_2\text{O}$ (0.4122 g / 50% organic solvent) to a 10 ml solution of the heptamolybdate (0.2672 g / 50% organic solvent). The hydrothermal synthesis assisted by microwaves was performed in an Anton Paar Monowave 300. The samples were subjected to different temperatures in a range of 90 to 180°C with a reaction time varying between 10 to 30 min under magnetic stirring. The synthesis temperature was controlled using an IR sensor that was calibrated using a ruby-based immersing fiber-optic probe and the rate of heating and temperature maintenance was controlled through the microwave irradiation power. The heating rate used was 100°C/min. After microwave treatment the collected slurry was centrifuged in a Sigma 2-16P centrifuge at 3500 rpm and the separated solid was washed twice with deionized water and absolute ethanol and finally dried for 8 h at 80°C in an oven. For comparison a $\text{Fe}_2(\text{MoO}_4)_3$ phase has been synthesized using a conventional precipitation-calcination protocol. This was done by mixing a solution of ammonium heptamolybdate with a solution containing iron nitrate nonahydrate in stoichiometric amount, keeping resulting precipitate under stirring for 1 hour. Next, the suspension was evaporated under vacuum at 40°C and then dried overnight at 120°C. Finally, the collected solid was calcined in air at 500°C for 3 hours. G-01 and -02 referred to samples respectively prepared with 10 and 30 min reaction time. The reaction temperature was also included in the name and specific value of other parameters given into brackets. For example, G-01-150(pH3) corresponds to a solid synthesized at 150°C for 10 min with a solution at pH=3.

In order to study the influence of the nature of the molybdenum precursor, solids were also prepared starting from molybdenum oxide. The MoO₃ phase precursor was obtained first by hydrothermal synthesis at 100°C for 40 min, following the procedure described in [18]. In this case a complete dissolution of the molybdenum oxide was not observed and the suspension was used as obtained for microwave irradiation.

Techniques used for the characterization of the catalysts

Iron and molybdenum metal contents of the catalysts have been determined by atomic absorption (ICP) in Argon plasma, using a SPECTROLAME-ICP, from SPECTRO. The solids (30-50 mg) were solubilized in an aqueous solution (100 ml) containing 5 ml of HF, H₂SO₄ and HNO₃ under stirring for 6 h at 473°C. The specific surface areas were measured using the BET method with liquid nitrogen adsorption at -196°C. Crystal structures of the phases obtained were controlled by X-ray diffraction using a BRUKER D5005 diffractometer and Cu K α radiation ($\lambda = 0.154184$ nm). Rietveld refinement of diffraction data was performed using Bruker Topas P program with March–Dollase equation for preferential orientation analysis of the textured samples. Scanning electron microscopy (SEM) has been performed using a JSM 5800LV (JEOL) microscope, coupled to an energy dispersion spectrometry (EDS) equipped with a diode Si-Li (PGT) for elemental analysis. The samples were also characterized by transmission electron microscopy (HRTEM) using a FEI TITAN ETEM G2 80–300 KV equipped with an objective Cs aberration corrector. Elemental chemical analyses were achieved in parallel using an EDX analyzer (SDD X-Max 80 mm² from Oxford Instruments). The HAADF–STEM images were acquired on a HAADF detector with a camera length such that the inner and outer cut-off half-angles of the detector were,

respectively, equal to 55 and 200 mrad. Mössbauer spectra of the prepared solids were recorded at room temperature using a 2 GBq $^{57}\text{Co}/\text{Rh}$ γ -ray source [19]. The accuracy of the fits was judged on the basis of fitting procedure conversion and χ^2 values.

X-ray photoelectron spectra (XPS) of the catalysts have been recorded after catalytic test using a KRATOS AXIS Ultra DLD spectrometer equipped with Al $K\alpha$ monochromatized source. Chemical states corresponding to Fe 2p, Fe 3p, Mo 3d, O 1s and C 1s levels were studied. The peaks were decomposed using combination of Voight functions with an overall FWHM of around 1.6 eV. Fe 3p signals were used to quantify iron species since core-hole relaxation effects in Fe 2p make it difficult to accurately determine the iron concentration.

Testing of the catalysts

The testing of the catalysts was conducted at 360°C with a gas feed composition $\text{C}_3\text{H}_6/\text{O}_2/\text{N}_2 = 1:1.5:8.6$, a total flow rate of 60 mL/min, and a catalyst mass of 140 mg in a fixed-bed down-flow reactor. The reaction products were analyzed online by injection of 1 mL of the gaseous mixture into a Shimadzu GC2014 Gas Chromatographer equipped with TCD and FID detectors. The quantification of N_2 , O_2 , C_3H_6 , CO, CO_2 and acrolein was performed on the TCD detector, whereas all the other oxygenated by-products were analyzed by the FID detector. The separation of the reaction products on the TCD line was carried out by means of two packed columns mounted in series: a Porapak Q (2 m, 80/100 mesh) and a molecular sieve (2m, 60/80 mesh), whereas the oxygenated products on the FID line were separated using a single capillary column Zebron-FFAP (30 m, 0.53 μm). CO_2 , CO, acrolein, acrylic acid and allyl alcohol were the principal reaction products, with carbon balance better than 98% [20].

RESULTS

Comparison between solids obtained with conventional and microwave heating

The physico-chemical properties of two different $\text{Fe}_2(\text{MoO}_4)_3$ phases, prepared by means of precipitation followed by conventional calcination, and microwave-assisted hydrothermal synthesis (MAHS), were compared (Fig.1, Table 1). The XRD patterns of the two solids were found to be comparable, and the cell parameters computed from the powder patterns were very similar, although slightly smaller in the case of the solids produced by microwave heating. This effect may arise from their lower crystallization temperature. In the case of the microwave-heated solid, its crystal size was also smaller, and its specific surface area (measured using the BET method) was correspondingly higher.

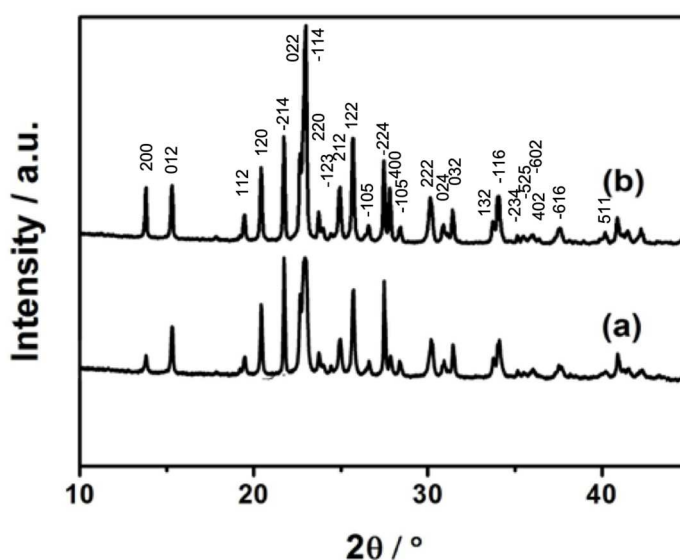


Figure 1. XRD patterns of $\text{Fe}_2(\text{MoO}_4)_3$ samples obtained by MAHS (a), and with the conventional precipitation-calcination reaction (b), indexation from JCPDS 00-035-0183.

Study of MAHS reaction parameters

In order to study the conditions under which the MAHS method could be used to obtain a crystalline phase of iron molybdate with a high specific surface area, the starting solution was subjected to two different reaction times (10 and 30 min), at six different temperatures ranging between 100 and 200 °C. Fig. 2 shows the XRD patterns obtained at each of these six temperatures, with 10 min reaction time, showing that a minimum of 120 °C was needed to obtain the crystallization of iron molybdate. As shown in Fig. 2, total crystallization appears to be achieved at around 150 °C.

Table 1. Main physico-chemical properties of the catalysts prepared using the MAHS reaction (sample a), and the classical method (sample b)

Parameters	Sample (a)	Sample (b)
Reaction time [min]	10	180
Reaction temperature [C°]	160	500
Cell parameters:		
a [nm]	1.57564	1.57632
b [nm]	0.92339	0.92373
c [nm]	1.82157	1.82320
β °	125.604	125.564
Crystal size [nm]	85	134
Surface area [m ² /g]	5.1	2.1

In parallel, the crystal size of the iron molybdate increased with reaction temperature, whereas its specific surface area decreased (Table 2). However, the reaction time did not appear to have any influence on the samples' crystallinity, crystal size or specific surface area (Table 2).

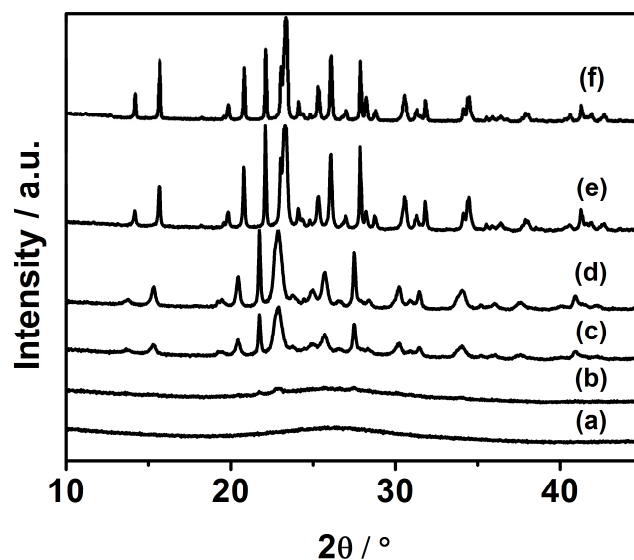


Figure 2. XRD patterns of the $\text{Fe}_2(\text{MoO}_4)_3$ samples, prepared at different temperatures using the MAHS method: 100°C (a), 110°C (b), 120°C (c), 130°C (d), 160°C (e), and 200°C (f).

Study of precursor solutions for the MAHS reaction

Influence of pH: In this set of tests, the samples were prepared using solutions at different values of pH. The pH of the mixed solutions was adjusted to pH=0.5, pH=3 and pH=5

Table 2. Crystal size (computed using XRD powder fitting) and specific surface area (determined using the BET method), for $\text{Fe}_2(\text{MoO}_4)_3$ samples.

Sample	Reaction time (min)	Temperature (°C)	Crystal size (nm)	Specific surface area (m^2/g)
G-01-100	10	100	-	-
G-01-110	10	110	32	33.0
G-01-120	10	120	38	16.2
G-01-130	10	130	46	7.2
G-01-160	10	160	85	5.1
G-01-200	10	200	136	3.1
G-02-120	30	120	40	15.8
G-02-130	30	130	47	5.6
G-02-160	30	160	88	4.3
G-02-200	30	200	139	3.0

respectively, using a solution of $\text{NH}_3\cdot\text{H}_2\text{O}$ 0.7445M and HNO_3 65%. All of the reactions for the study of the influence of pH were carried out for 10 minutes at 150 °C. Fig. 3 shows the resulting XRD patterns obtained with the $\text{Fe}_2(\text{MoO}_4)_3$ samples, which appear to be similar, although the relative intensities of several peaks were found to vary with increasing pH. Similar features were better observed when the molybdenum precursor was changed, as discussed in the following section. Increasing pH was found to promote an increase in crystal size, and the highest solid yield was obtained at pH=3 (Table 3).

Table 3. Display data of the three samples of $\text{Fe}_2(\text{MoO}_4)_3$ at different pH.

Sample	pH	Crystal-size from	Yield
G-01-150(pH0.5)	0.5	63.6	75
G-01-150(pH3)	3	100	90
G-01-150(pH5)	5	115	70

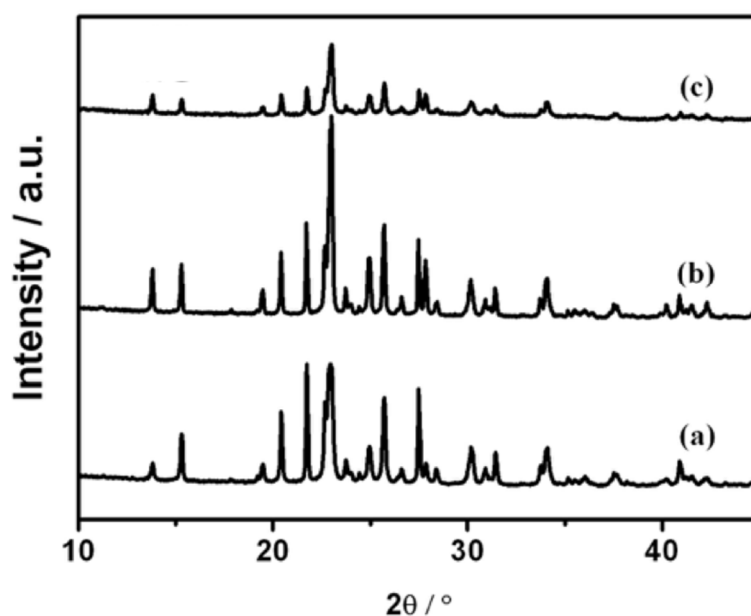


Figure 3. XRD patterns of $\text{Fe}_2(\text{MoO}_4)_3$ prepared using solutions at pH=0.5 (a), pH=3 (b) and pH= 5 (c).

Influence of the addition rate of the metallic salts: Three samples were synthesized using different rates for the addition of iron nitrate to the heptamolybdate solution (1, 3 and 5 ml/min). The results shown in Table 4 reveal only small differences in crystal size, surface area and Fe₂(MoO₄)₃ yield. In addition, the XRD patterns obtained with these samples were very similar. This parameter thus appears to be of little significance in terms of the resulting morphology of the iron molybdates.

Table 4. Influence of the rate of addition of metallic salts to the starting solution in the synthesis of iron molybdate.

Sample	Addition rate [ml/min]	Crystal size [nm]	Surface area [m ² /g]	Yields [%]
G-01-130(1ml)	1	46	7.2	90
G-01-130(3ml)	3	44	7.9	92
G-01-130(5ml)	5	42	8.4	94

Influence of the nature of the molybdenum precursor: In order to study the influence of the nature of the molybdenum precursor, molybdenum oxide was used as the starting material, instead of ammonium molybdate. With MoO₃, pure phases of iron molybdate were obtained after 30 min at 200 °C, as in the case of ammonium heptamolybdate. A strong preferential orientation was however detectable by XRD (Fig. 4).

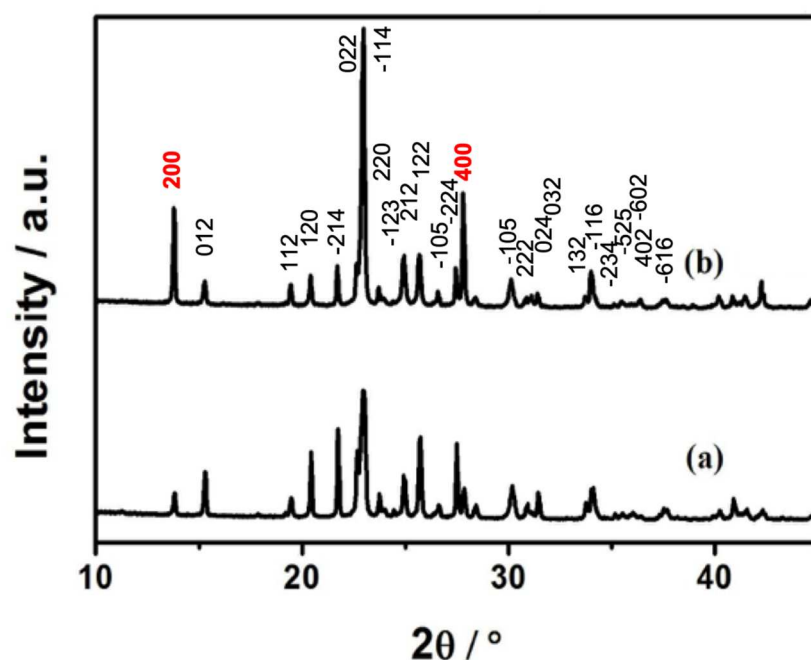


Figure 4. XRD patterns of $\text{Fe}_2(\text{MoO}_4)_3$ prepared using as the molybdenum precursor ammonium heptamolybdate (a) and MoO_3 (b). indexation from JCPDS 00-035-0183. Peaks which increased intensity are marked in red.

SEM analysis confirmed this observation, revealing significant differences between the morphologies of the samples prepared with ammonium heptamolybdate. The latter sample presented sphere-like agglomerates of platelets, forming relatively uniformly sized “rosettes”, which to a certain extent are comparable to those obtained with VPO catalysts (Fig.5a) [21]. When MoO_3 was used, the samples’ morphology was characterized by larger, well-defined and non-agglomerated crystal plates, which were found to have mainly perpendicular twinning and to form small clumps (Fig. 5c and d) [22]. These clumps were occasionally associated with some particles of few hundreds of nanometers without specific form.

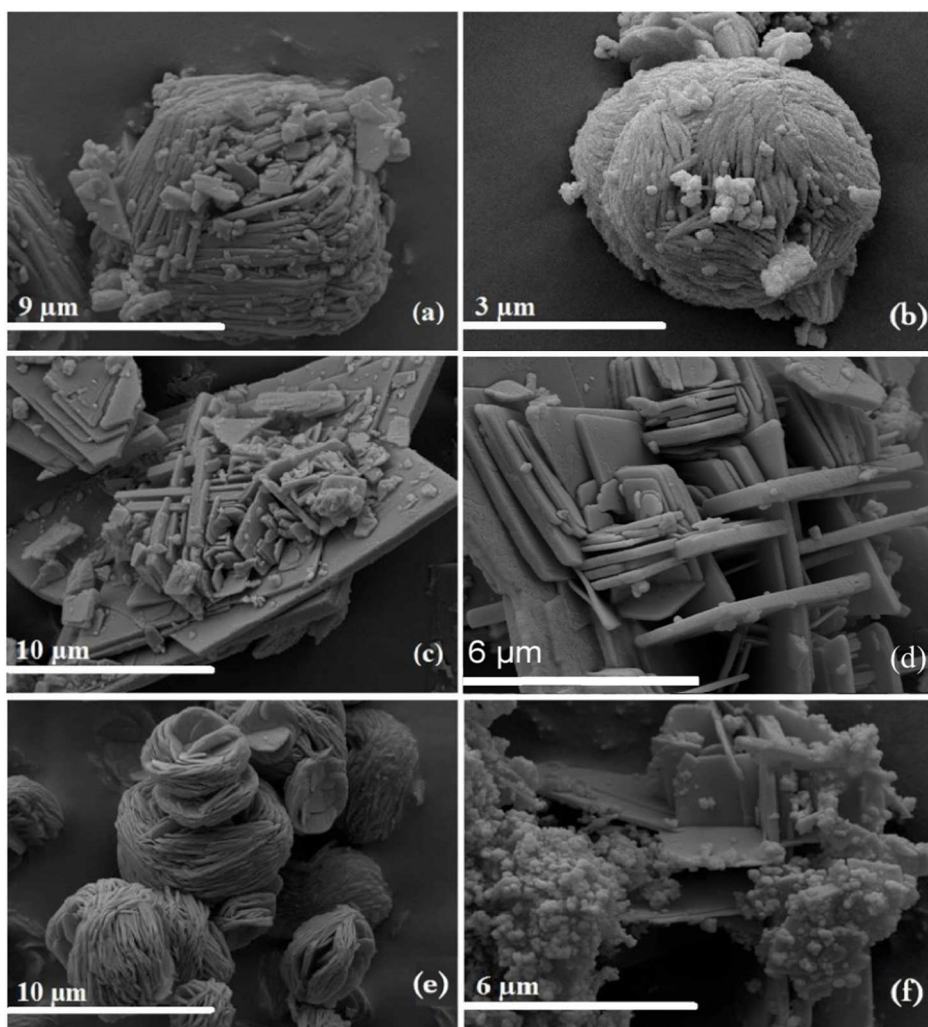


Figure 5. SEM images of $\text{Fe}_2(\text{MoO}_4)_3$, synthesized with ammonium heptamolybdate at 200 °C (a) and at 150 °C (b), $\text{Fe}_2(\text{MoO}_4)_3$ synthesized with MoO_3 at 200 °C (c and d) and $\text{Fe}_2(\text{MoO}_4)_3$ synthesized with ammonium heptamolybdate in an ethanol/water solution at 130 °C, (e) and at 150 °C (f).

In order to gain better insight into the preferential orientation of the solid prepared using MoO_3 , the powder patterns of both phases were studied using Rietveld analysis. The resulting Rietveld plots are shown in Fig. 6. The best fit for the powder pattern obtained from the sample prepared with MoO_3 showed a strong preferential orientation in the $[1\ 0\ 0]$ direction. In the case of the solid prepared using ammonium heptamolybdate, a slight orientation in the $[1\ 0\ 0]$ and $[1\ -1\ 2]$ directions, was observed. No significant difference was detected in the cell parameters.

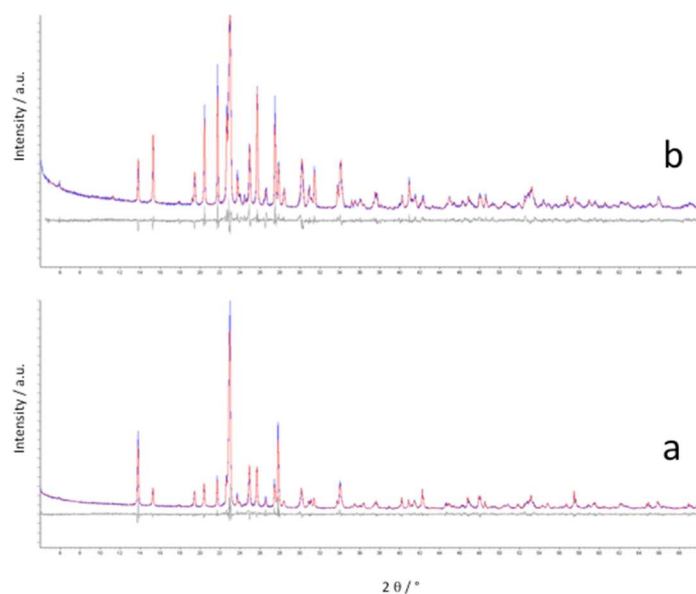


Figure 6. Observed (blue) and calculated (red) powder XRD pattern profiles and difference plot [$(I_{\text{obs}} - I_{\text{calc}})$] (grey) of the Rietveld refinement of samples prepared using MoO_3 (a) and $(\text{NH}_4)_6\text{Mo}_7\text{O}_{24}$ (b), and collected at room temperature.

The fit of the powder pattern of the sample prepared with MoO_3 showed a strong preferential orientation in the [1 0 0] direction. For the solid prepared using ammonium heptamolybdate a slight orientation in [1 0 0] and [1 -1 2] direction was observed. No significant difference in cell parameters was detected.

Influence of the nature of the solvent: Iron molybdate catalyst synthesis was tested using four different solvents: water, ethylene glycol, 2-methylpropan-1-ol and ethanol. The organic solvents were mixed with water, at a 1:1 ratio. Samples were then synthesized at 130 °C and 150 °C, for 10 minutes. All of the XRD patterns obtained for the resulting solids, as well as their morphologies, were comparable, with the exception of the solid prepared in a water-ethanol mixture at 150°C, which showed a preferential orientation similar to that observed when MoO_3 was used as the molybdenum precursor (Fig. 7). This result was expected, and

can be explained by the presence of platelets in the sample, as observed by SEM (Fig. 5f). The platelets were however smaller, and embedded within clusters of other particles. At lower temperatures, the solid maintained the rosette-like morphology shown in Fig. 5e.

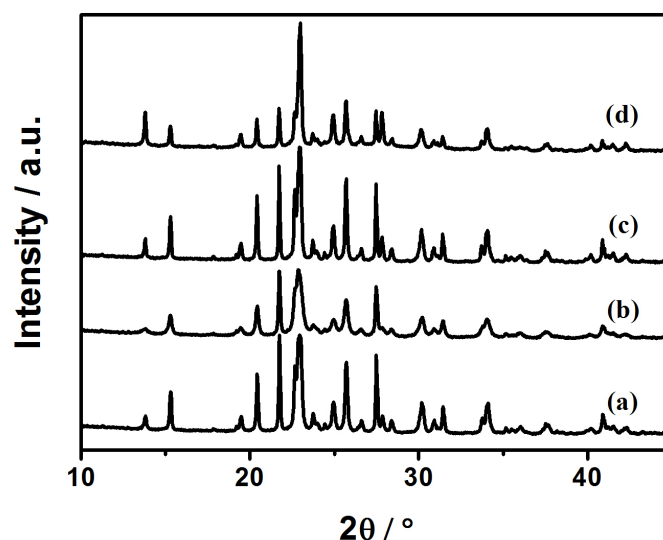


Figure 7. XRD patterns of $\text{Fe}_2(\text{MoO}_4)_3$ prepared using different solvents, mixed at a 1:1 ratio with water, corresponding to: (a) water only, (b) ethylene glycol, (c) 2-methylpropan-1-ol, (d) ethanol.

It was important to verify that any differences in morphology were not associated with the presence of structural defects. Ferric molybdate is known to undergo local sub-stoichiometry, which can be revealed using EPR or Mössbauer spectroscopy [23]. For this reason, we characterized the solids using Mössbauer spectroscopy (Fig. 8). All the resulting spectra were quite similar, with only one doublet, an isomeric shift of $\delta=0.39\pm 0.02$ mm/s, and quadrupolar splitting $\Delta=0.21\pm 0.02$ mm/s corresponding to pure $\text{Fe}_2(\text{MoO}_4)_3$ [8,23]. It was thus possible to conclude that none of the observed changes in morphology involved structural defects that could have altered the properties of the solids.

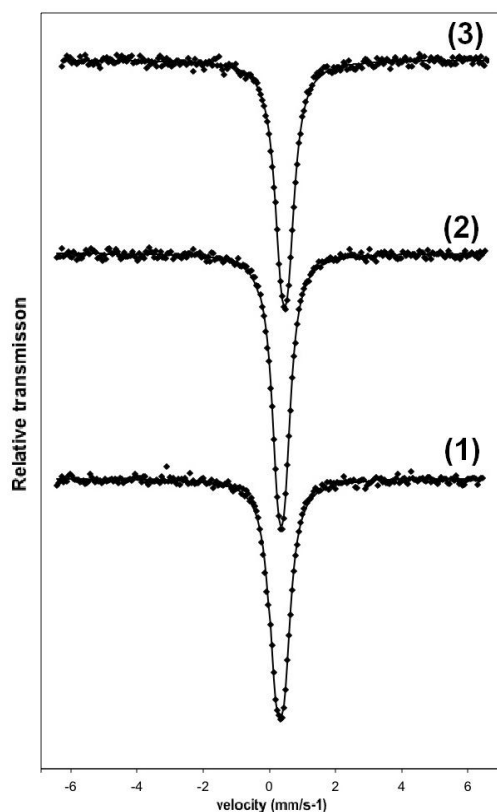


Figure 8. Mössbauer spectra of iron molybdate with: ammonium heptamolybdate in water (1), MoO_3 in water (2) and ammonium heptamolybdate in a mixed ethanol/water solvent (3); the continuous lines are derived from a least-squares fit to the data.

Catalytic testing of the synthesized iron molybdates

The two catalysts synthesized at 200°C for 30 min, using ammonium heptamolybdate and MoO_3 as precursors, were tested under the same conditions as described in the experimental section. These were chosen in order to ensure low conversion, and to allow the catalysts' initial rates of conversion and selectivity to be computed and compared. Both catalysts were subjected to a deactivation process, allowing their catalytic properties to be stabilized after approximately 70 hours of operation. Similarly to previous reports on molybdate catalyst behavior [20,24], the samples tested in the present study exhibited simultaneous variations in selectivity, with a decrease in the formation of deep oxidation products and an almost equivalent gain for acrolein. This deactivation can be explained by sintering of the $\text{Fe}_2\text{Mo}_3\text{O}_{12}$

phase under catalytic reaction conditions, which leads to a reduction in its specific surface area. In the present study, the specific surface area of the solid prepared with heptamolybdate decreased from 16.1 to 9.9 m²/g, and that of the solid prepared with MoO₃ decreased from 4.1 to 2.6 m²/g. On the other hand, concomitant molybdenum enrichment of the amorphous surface layer, together with the suppression of some of the iron acid sites responsible for deep oxidation at the surface, have been proposed as an explanation for the observed increase in selectivity [24].

The catalytic properties of the two solids, after stabilization, are listed in Table 5. This comparison shows that the morphology of the samples has a significant influence on their catalytic properties. The solids prepared with MoO₃ and having a preferential orientation had a higher intrinsic activity, and a higher selectivity to acrolein and allyl alcohol, than the samples prepared with ammonium molybdate.

Table 5. Catalytic properties of the samples prepared using different molybdenum precursors tested at 360 °C, with a gas feed composition adjusted to: C₃H₆/O₂/N₂ = 1:1.5:8.6, a total flow rate of 60 mL/min, and a catalyst mass of 140 mg after 70 h on stream.

Mo precursor	Conv. (%)	Rate of propene conv. (10 ⁻⁸ mol.s. ⁻¹ m ²)	Selectivity (%)			
			Acr	AlA	CO ₂	CO
(NH ₄) ₆ Mo ₇ O ₂₄	1.0	2.9	75.2	0.1	15.9	5.6
MoO ₃	0.8	9.0	89.7	0.6	4.6	0.3

During the course of this study, it was important to assess any difference in surface composition between the two types of solid, which could explain the observed differences in catalytic properties. In this respect, the Fe₂Mo₃O₁₂ phase has been shown by many authors to be covered by a layer of molybdenum oxide, and that this layer, which is amorphous, corresponds to the active phase of the catalysts [25-28]. The samples were analyzed using

high-resolution transmission electron microscopy (HRTEM), with the resulting images systematically revealing an amorphous layer coating the crystalline bulk, at the surface of both samples (Fig. 10). This layer was about 5 nm thick on the sample prepared with MoO_3 , and 3 nm thick on the sample prepared with ammonium molybdate. In contrast to previous interpretations, our EDX analyses indicate that although the amorphous layer contained some iron, it appeared to be much richer in molybdenum than the bulk material. These analyses revealed comparable Fe/Mo ratios for both compounds, i.e. 0.41 ± 0.10 and 0.39 ± 0.15 , for the samples prepared with MoO_3 and ammonium molybdate, respectively. It was carefully verified that amorphous layers were present on all facets of these particles (Fig. 9).

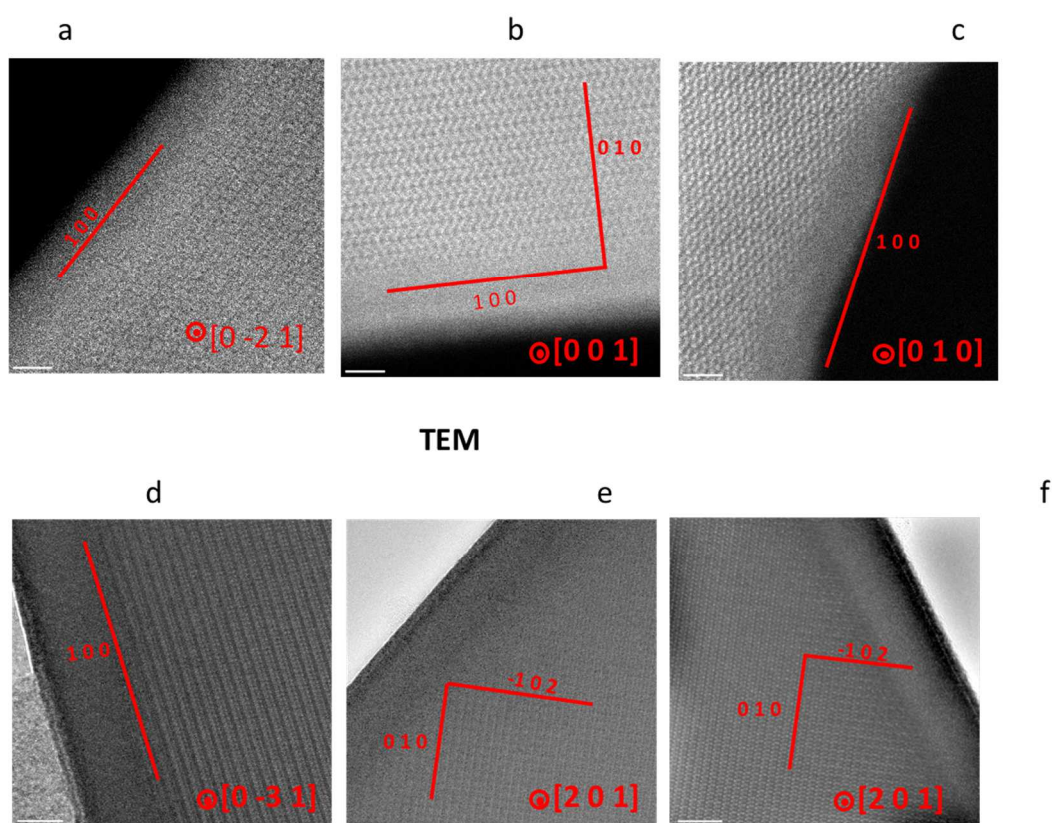


Figure 9. High-resolution STEM-HADF images of the samples prepared with ammonium heptamolybdate (a, b, c) and MoO_3 (c, d, e), showing the projection, in various directions, of the structures with the amorphous layers.

X-ray photoelectron spectroscopy (XPS) analyses were also performed on the solids, following the catalytic tests (Table 6). Two molybdenum signals were present, with binding energies of 232.4 and 231.7 eV (Mo3d5/2 peak) respectively, characteristic of the Mo(VI) and Mo(V) species [29,30]. Similarly for iron, two signals were observed with binding energies of 711.5 and 709.8 eV, which are characteristic of the Fe2p3/2 peak of the Fe(III) and Fe(II) species [31,32]. The atomic concentrations of these species were comparable for both solids. Over the full extent of the amorphous layer, the surface Fe/Mo ratios appeared to be slightly higher than those measured by EDX.

Table 6. Results of the XPS analysis of the catalysts prepared using different molybdenum precursors, tested at 360 °C with a gas feed composition adjusted to: C₃H₆/O₂/N₂ = 1:1.5:8.6, a total flow rate of 60 mL/min, and a catalyst mass of 140 mg after 70 h on stream.

Precursor	Fe binding energy (eV).		Mo binding energy (eV)		Relative concentration		
	Fe ²⁺ /Fe _{tot}	Mo ⁵⁺ /Mo _{tot}	Fe ²⁺ /Fe _{tot}	Mo ⁵⁺ /Mo _{tot}	Fe ²⁺ /Fe _{tot}	Mo ⁵⁺ /Mo _{tot}	Mo ⁵⁺ /Mo _{tot}
(NH ₄) ₆ Mo ₇ O ₂₄	711.5	709.4	232.4	231.7	0.08	0.17	0.54
MoO ₃	711.4	709.4	232.4	231.6	0.10	0.19	0.53

DISCUSSION

The results of this study show that microwave-assisted hydrothermal synthesis (MAHS) can easily be used to prepare Fe₂(MoO₄)₃ catalysts, and that with optimized parameters it is possible to obtain a single, well-crystallized phase with a specific surface area as high as 15 m²/g. This specific surface area is greater than that, which is generally obtained using the conventional precipitation-calcination method. Most of the test parameters had no significant influence on the crystallization of ferric molybdate, with the exception of the reaction temperature, which needed to be greater than or equal to 120 °C. Different results could have

been expected when the pH of the solution was varied between 0.5 and 5, since over this range of acidities the distribution of molybdenum species is known to vary, with a high probability for the formation of several specific polynuclear anionic species, such as $\text{Mo}_7\text{O}_{23}\text{OH}^{5-}$, $\text{Mo}_7\text{O}_{22}(\text{OH})_2^{4-}$ and $\text{Mo}_7\text{O}_{21}(\text{OH})_3^{3-}$ [33]. However, in the present study, the pH did not appear to influence the properties of the ferric molybdate crystallized under irradiation.

On the other hand, the nature of the molybdenum precursor used to produce the catalysts appears to have a drastic effect on the morphology of the synthesized iron molybdate. Although the catalyst prepared using ammonium heptamolybdate presented with a “rosette” type of spherical, agglomerated platelets, the catalyst prepared with MoO_3 exhibited large, well-defined crystal plates (Fig. 5). These plates also account for a large proportion of the solid when an ethanol-water mixture is used, with a reaction temperature equal at least to 150 °C (Fig. 5d). These morphologies go hand in hand with the observation (using XRD) of a preferential structural orientation of the samples in the (100) direction.

We hypothesize that this specific morphology is related to the presence of MoO_3 as a phase, during microwave irradiation, which first has to solubilize before it can react with iron. This dissolution restrains the molybdenum concentration in the solution, thus influencing the growth of $\text{Fe}_2\text{Mo}_3\text{O}_{12}$ particles, which takes place in their preferential direction of growth, along the [-102] axis, leading to the formation of large platelets (Fig. 5c). This phenomenon can also explain the behavior observed when an ethanol-water mixture is used as a solvent, at 150 °C even though ammonium heptamolybdate is the molybdenum precursor. In this case, the presence of ethanol triggers the partial precipitation of MoO_3 during heating, prior to its reaction with the iron precursor, thus leading to a situation similar to that observed in the

previously described one with the formation of large platelets. Interestingly, when ammonium heptamolybdate alone is microwave heated, for 10 min at 130 °C in an ethanol-water mixture, no precipitation occurs, whereas significant precipitation ensues at 150 °C under the same conditions. This would explain why the classical expected morphology is obtained at 130 °C.

The development of large platelets in the solid prepared using MoO₃ leads to both high intrinsic activity, and high selectivity to acrolein. Since this solid was characterized by an increased exposure of its *ac* planes, it is possible that the most active and selective sites for propene oxidation to acrolein are situated on the (010) crystallographic surface. In the presence of rosette morphology, these planes are not so well developed and partially obscured which would explain the lower activity. Interestingly, the same observation was made in the case of VPO catalysts, when solids with similar morphologies were compared [28]. However, contrary to the case of VPO catalysts, the TEM characterization of ferric molybdate catalysts in the present study shows that in both cases, all facets of the solid's particles, including that corresponding to the (010) planes, were covered by an amorphous layer and a direct crystal structure activity relation cannot be similarly established. This amorphous layer has exactly the same composition on all facets, with only small variations in thickness being found from one sample to another (± 3 nm). These features make it possible to eliminate variations in structure and stoichiometry as potential explanations for the specific properties of the active, exposed surfaces. One of the few remaining possibilities is that the structure of the bulk crystallized phase, which behaves as a support, modifies the properties of the supported amorphous phase. By focusing our attention on the structure of the Fe₂(MoO₄)₃ phase, it can be understood that this corresponds to a low packing density of FeO₆ octahedra and MoO₄ tetrahedra, joined together at their apexes, with two channel-like cavities extending, perpendicular to the (010) planes. Fig. 10 provides a schematic representation of the structure,

in which both types of channel have been marked with the letters S and T, as in the initial publication describing the structure of iron molybdate [34]. These channels would allow the diffusion of oxygen anions from the bulk to the catalytic amorphous layer, and lead to faster re-oxidation of the catalytic sites at the surface of the amorphous layer on the (010) plane. The limiting rate of the catalytic reaction, which on this type of compound occurs via the Mars-van Krevelen mechanism at 360 °C, is the re-oxidation of the catalyst. This might provide an explanation for the catalysts with a platelet morphology having a much higher activity, and an increased selectivity. Indeed, on this type of catalyst the selectivity was highly dependent on the oxidation state of the surface. The more the phase being oxidized more selective were the catalytic sites. A very similar example is provided by the case study of multi-component BiFeCoMoO catalysts, although in this case the diffusion of oxygen, which increases the oxidation state of the active $\text{Bi}_2\text{Mo}_3\text{O}_{12}$ phase, was driven by another phase, corresponding to a mixed iron and cobalt molybdate in close interaction with the active phase. This also led to an increase in activity and selectivity [35, 36].

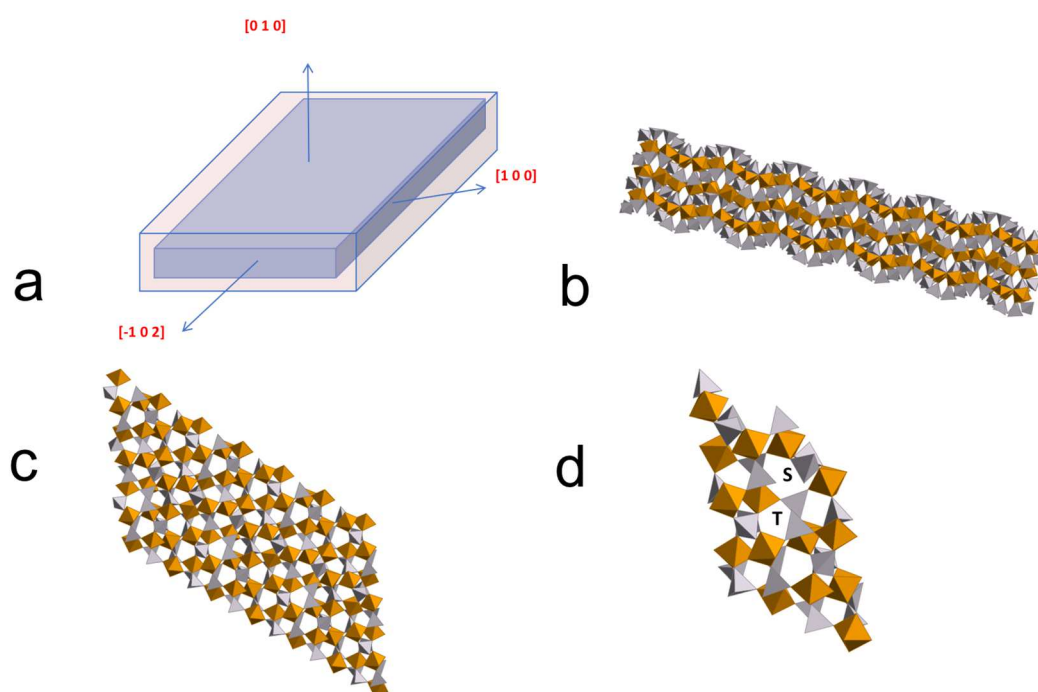


Figure 10 Schematic representation, $\text{Fe}_2(\text{MoO}_4)_3$ platelets (a) with structure built using FeO_6 octahedra and MoO_4 tetrahedra, in the [001] direction (b), showing the stacking of chains and layers, and in the [010] direction (c), with an enlargement showing two different types (S and T) of channel-like cavity (d).

CONCLUSION

This study demonstrates that the MAHS method is well-suited to the synthesis of iron molybdate catalysts, and can be used to control the size and shape of the resulting particles. The successful synthesis of a pure phase of iron molybdate can be achieved between 150 °C and 200 °C, following a reaction time as short as 10 minutes, with a yield as high as 94% being achieved by adjusting the addition rate of the precursor solution to 5 ml/min, and maintaining its pH in the range between 1 and 3. Different iron molybdate morphologies can be obtained by changing the molybdenum precursor from ammonium heptamolybdate to molybdenum oxide, or by using water-ethanol mixtures as the solvent during MAHS synthesis. This outcome is explained by the presence of either residual, or new MoO_3 during the reaction, which in some way buffers the Mo concentration in the liquid phase, thus promoting crystal growth through the plane, with a balanced iron and molybdenum content, i.e. (-102) and (100) faces.

Although the surface structure and composition of both solids correspond to an amorphous layer, and appear to remain unchanged, other morphological changes in the catalysts are shown to have a significant influence on their catalytic properties. We propose that the catalytic sites on the amorphous layer, situated on the (100) planes, are more easily re-oxidized due to the faster diffusion of oxygen anions in the perpendicular structure channels. Since the catalyst re-oxidation is the limiting reaction step, this would explain why

the catalysts with platelets morphology are more active. At steady state, the considered active sites would not only be more numerous but also with a change in nature like that would explain the increase in selectivity like in the case of $\text{Bi}_2\text{Mo}_3\text{O}_{12}$ in multicomponent catalysts.

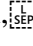
The present study provides an example of molybdate structure sensitivity in an oxidation reaction, despite the formation of an amorphous layer covering the entire surface of the crystalline phase particles. This outcome again emphasizes the fact that bulk-surface interactions play a crucial role in the catalytic activity of oxide catalysts, and that appropriate control of these interactions can be used to optimize the development of new, efficient catalysts.

REFERENCES

- [1] H. Adkins, W.R. Peterson, The oxidation of methanol with air over iron, molybdenum and iron-molybdenum oxides, *J. Am. Chem. Soc.* 53 (1931) 1512-1520.
- [2] G. Reuss, W. Diesteldorf, A.O. Gamer, A. Hilt, *Ullmans Encycl. Ind. Chem.* (2002).
- [3] P. Forzatti, P.L. Villa, N. Ferlazzo, D. Jones, Multicomponent catalysts for the oxidation of propylene to acrolein: $\text{Fe}_2(\text{MoO}_4)_3$ doped with Bi or Te, *J. Catal.* 76 (1982) 188-207.
- [4] W. Ueda, Y. Moro-oka, T. Ikawa, Role of transition metal elements in Te-Mo-O catalysts as revealed by the oxidation of propylene to acrolein with O_2 tracer, *Chem. Lett.* 11 (1982) 483-486.

- [5] L. Zhang, X.-F. Cao, Y.-L. Ma, X.-T. Chen, Z.-L. Xue, Pancake-like $\text{Fe}_2(\text{MoO}_4)_3$ microstructures: Microwave-assisted hydrothermal synthesis, magnetic and photocatalytic properties, *New J. Chem.* 34 (2010) 2027-2033.
- [6] D. Li, J. Xue, M. Liu, Synthesis of $\text{Fe}_2(\text{MoO}_4)_3$ Microspheres by self-assembly and photocatalytic performances, *New J. Chem.* 39 (2015) 1910-1915.
- [7] L.E. Briand, A.M. Hirt, I.E. Wachs, Quantitative Determination of the Number of Surface active Sites and the Turnover Frequencies for Methanol Oxidation over Metal Oxide Catalysts: Application to Bulk Metal Molybdates and Pure Metal Oxide Catalysts, *J. Catal.* 202 (2001) 268-278.
- [8] A.P.V. Soares, M. Farinha Portela, A. Kiennemann, L. Hilaire, J.M.M. Millet, Iron molybdate catalysts for methanol to formaldehyde oxidation: effects of Mo excess on catalytic behavior, *Appl. Catal. A: Gen.* 206 (2001) 221-229.
- [9] J.C. Volta, J.L. Portefaix, Structure sensitivity of mild oxidation reactions on oxide catalysts - a review, *Appl. Catal.* 18 (1985) 1-32.
- [10] J.C. Volta, B. Moraweck, Specificity of MoO_3 crystalline faces in propene oxidation, *J. Chem. Soc. Chem. Comm.* (1980) 338-339.
- [11] J.-C. Volta, M. Forissier, F. Theobald, T.P. Pham, Dependence of selectivity on surface structure of MoO_3 catalysts, *Faraday Discuss. Chem. Soc.* 72 (1981) 225-233.
- [12] M. Abon, J. Massardier, B. Mingot, J.C. Volta, N. Floquet, O. Bertrand, New unsupported [100]-oriented MoO_3 catalysts II. Catalytic properties in propylene oxidation, *J. Catal.* 134 (1992) 542-548.

- [13] J.C. Vedrine, G. Coudurier, J.M.M. Millet, Molecular design of active sites in partial oxidation reactions on metallic oxides, *Catal. Today* 33 (1997) 3-13.
- [14] J.M. Tatibouet, C. Phichitkul, J.E. Germain, 14 Structure-sensitive catalytic oxidation of butenes on molybdenum trioxide crystallites, *J. Catal.* 99 (1986) 231-234.
- [15] E.M. Gaigneaux, H.M. Abdel Dayem, E. Godard, P. Ruiz, Dynamic phenomena and catalytic reactivities of oxide surfaces, *Appl. Catal. Gen.* 202 (2000) 265-283.
- [16] J.M. Tatibouët, J.E. Germain, *J. Catal.* 72 (1981) 375–378.
- [17] K. Schuh, W. Kleist, M. Høj, A.D. Jensen, P. Beato, G.R. Patzke, J.D. Grunwaldt, J. Systematic study on the influence of the morphology of α -MoO₃ in the selective oxidation of propylene, *Solid State Chem.* 228 (2015) 42-52.
- [18] X.W. Lou, H.C. Zeng, Hydrothermal Synthesis of α -MoO₃ Nanorods via Acidification of Ammonium Heptamolybdate Tetrahydrate, *Chem. Mater.* 14 (2002) 4781-4789.
- [19] J.M.M. Millet, C. Virely, M. Forissier, P. Bussière, J.C. Vedrine, Mössbauer spectroscopic study of iron phosphate catalysts used in selective oxidation, *Hyperfine Interact.* 46 (1989) 619-628.
- [20] M. Tonelli, L. Massin, L. Cardenas, F. Ivars-Barcelo, V. Belliere Baca, J.M.M. Millet, Cooperation between redox couples at the surface of molybdates based catalysts used for the selective oxidation of propene, *J. Catal.* *accepted for publication* (2019).
- [21] H.S. Horowitz, C.M. Blackstone, A.W. Sleight, G. Teufer, V-P-O catalysts for oxidation of butane to maleic anhydride : Influence of (VO)₂H₄P₂O₉ precursor morphology on catalytic properties *Appl. Catal.* 38 (1988) 193-210.

- [232] H. Chen, The Crystal Structure and Twinning Behavior of Ferric Molybdate $\text{Fe}_2(\text{MoO}_4)_3$, Mater. Res. Bull. 14 (1979) 1583-1590.
- [23] S. Angelov, in: N. Yordanov, World Scientific, London, Pravatz-Bulgaria, 1989, p. 359.
- [24] M. Tonelli, M. Aouine, L. Massin, V. Belliere Baca and J.M.M. Millet, Selective oxidation of propene to acrolein on FeMoTeO catalysts: determination of active phase and enhancement of catalytic activity and stability, Catal. Sci. Technol. 7 (2017) 4629-4639.
- [25] K. Routray, W. Zhou, C. J. Kiely, W. Grünert and I. E. Wachs, Origin of the synergistic interaction between MoO_3 and iron molybdate for the selective oxidation of methanol to formaldehyde, J. Catal., 2010, 275, 84.
- [26] E. Söderhjelm, M. P. House, N. Cruise, J. Holmberg, M. Bowker, J. O. Bovin and A. Andersson, On the Synergy Effect in MoO_3 - $\text{Fe}_2(\text{MoO}_4)_4$ Catalysts for Methanol Oxidation to Formaldehyde, Top. Catal., 2008, 50, 145-155.
- [27] C. Brookes, P.P. Wells, N. Dimitratos, W. Jones, E.K. Gibson, D.J. Morgan, G. Cibin, C. Nicklin, D. Mora-Fonz, D.O. Scanlon,  C.R.A. Catlow, and M. Bowker, Molybdenum Oxide on Fe_2O_3 Core-Shell Catalysts: Probing the Nature of the Structural Motifs Responsible for Methanol Oxidation Catalysis, J. Phys. Chem. C 118 (2014) 26155-26161.
- [28] C. Brookes, P.P. Wells, N. Dimitratos, W. Jones, E.K. Gibson, D.J. Morgan, G. Cibin, C. Nicklin, D. Mora-Fonz, D.O. Scanlon, C.R.A. Catlow, M. Bowker, The Nature of the Molybdenum Surface in Iron Molybdate. The Active Phase in Selective Methanol Oxidation, J. Phys. Chem. C 118 (2014) 26155-26161.

- [29] J. Baltrusaitis, B. Mendoza-Sanchez, V. Fernandez, R. Veenstra, N. Dukstiene, A. Roberts, N. Fairley, Generalized Molybdenum Oxide Surface Chemical State XPS Determination via Informed Amorphous Sample Model. *Appl. Surf. Sci.* 326 (2015) 151-161.
- [30] C.V. Ramana, V.V. Atuchin, V.G. Kesler, V.A. Kochubey, L.D. Pokrovsky, V. Shutthanandan, U. Becker, R.C. Ewing, Growth and Surface Characterization of Sputter-deposited Molybdenum Oxide thin Films. *Appl. Surf. Sci.* 253 (2007) 5368-5374.
- [31] A.P.S. Dias, F. Montemor, M.F. Portela, A. Kiennemann, The Role of the Supra-Stoichiometric Molybdenum during Methanol to Formaldehyde Oxidation over Mo-Fe mixed Oxides. *J. Mol. Catal. Chem.* 397 (2015) 93-98.
- [32] K. Thavornprasert, M. Capron, L. Jalowiecki-Duhamel, O. Gardoll, M. Trentesaux, A.S. Mamede, G. Fang, J. Faye, N. Touati, H. Vezin, J.L. Dubois, J.L. Couturier, F. Dumeignil, Highly Productive Iron Molybdate Mixed Oxides and their Relevant Catalytic Properties for Direct Synthesis of 1,1-dimethoxymethane from Methanol. *Appl. Catal. B: Env.* 145 (2014) 126-135.
- [33] Olazabal, M.A., Orive, M.M., Fernandez, L.A., Madariaga, J.M., 1992. Selective extraction of vanadium (V) from solutions containing molybdenum (VI) by ammonium salts dissolved in toluene. *Solvent Extraction and Ion Exchange* 10 (4), 623-635.
- [34] M.H. Rapposch, J.B. Anderson, E. Kostiner, Crystal Structure of Ferric Molybdate, $\text{Fe}_2(\text{MoO}_4)_3$, *Inorg. Chem.* 19 (1980) 3531-3539.
- [35] Y. Moro-Oka, D.-H. He and W. Ueda, Catalytic oxide support oxide interaction to prepare multifunctional oxidation, (R.K. Grasselli and A.W. Sleight Edts) *Stud. Surf. Sci. Catal.*, 67 (1991) 57-61.

[36] J.M.M. Millet, H. Ponceblanc, G. Coudurier, J.M. Herrmann, J.C. Vedrine, Study of multiphasic molybdate based catalysts. II Synergy effect between bismuth molybdates and mixed iron and cobalt molybdates in mild oxidation of propene. *J. Catal.* 142 (1993) 381-391.

